

PARAMETER OPTIMIZATION OF PROPORTIONAL INTEGRAL CONTROLLER IN THREE-PHASE FOUR-WIRE GRID-CONNECTED INVERTER USING ANT COLONY OPTIMIZATION

^{1,2}SUSATYO HANDOKO, ¹SASONGKO P. HADI, ¹SUHARYANTO, ¹EKA FIRMANSYAH

¹Department of Electrical Engineering and Information Technology, UGM, Yogyakarta, Indonesia

²Department of Electrical Engineering, Diponegoro University, Semarang, Indonesia

E-mail: susatyo_s3_09@mail.ugm.ac.id, sasongko@te.ugm.ac.id, suharyanto@ugm.ac.id, eka.firmansyah@ugm.ac.id

ABSTRACT

This paper presents the parameter optimization of proportional integral (PI) controller in four-leg inverter for DG application when installed in a three-phase four-wire distribution system. The inverter can be utilized as power converter to inject power generated from renewable source to the grid and as shunt active power filter to compensate load current harmonics, load reactive power demand, and current unbalance. To achieve those functions, a reference current needs to be determined. In this study, DC voltage regulator used PI controller to generate the peak value of reference grid current. Optimal tuning of PI gain was required to obtain the best performance of PI controller. An algorithm based on the ant colony optimization (ACO) method was used to optimize the PI parameters. The objective function of optimization was to minimize the integral time absolute error (ITAE) of dc-link voltage and average total harmonic distortion of grid currents ($THDi_{ave}$). The usefulness of the approach was demonstrated by a simulation.

Keywords: *Grid-Connected Inverter, PI Controller, ACO, ITAE, THDi*

1. INTRODUCTION

For many years, fossil fuels have been the primary source of the energy and supply about 75 percent of total global energy demand. The increase of world energy demand, air pollution, global warming, and extinction of fossil fuels have made it necessary to consider renewable sources as a future energy solution. In recent years, the interest in using renewable energy for power generation in many countries has rapidly increased.

DG sources such as wind, photovoltaic (PV), micro turbines and fuel cells are being connected rapidly to the electricity network. Most of DG units are interfaced with the utility through power electronics, which facilitate the operation and control of DGs. Many control strategies for grid-connected inverter have now been introduced [1]-[7]. Some of them use four-leg inverter [5]-[7]. A number of different control strategies have been introduced over the last few years such as: predictive controls [1], [2], hysteresis controls [3], [7], and power balance controls [4]-[6]. A method to select the bandwidth of hysteresis band optimally

has also been presented [3]. The power balance strategy is one of control techniques, which are used to control the injected power in the inverter for DG application [4]-[6].

In the grid connected mode, it is important to regulate the output current and to improve the dynamic response of the grid. The appropriate parameters of controller enable to enhance the system stability and achieve ideal dynamic response characteristics. However, studying on how to select the parameters is deemed essential.

A number of researches about parameters optimization for inverter, in essence, have been introduced as in active power filter [8], [9] and DG application [10]-[12]. The comparative study of PI controller tuning in SAPF using three evolutionary algorithms has been presented. The objective functions for optimization include integral time square error (ITSE) and integral time absolute error (ITAE) [8]. The different operating conditions such as weak or strong AC system here are considered for optimization [10]. A control technique-based PQ control is used to inject predefined active and reactive powers to utility. The controller parameters

are designed optimally to improve the stability response of the microgrid [12].

In this paper, an optimal method for tuning the PI parameters in DC voltage regulator of grid-connected inverter system is presented. Recently, ant colony algorithm is applied in various fields, such as power grid planning, control system parameter optimizing and constrained load flow problem. This paper proposed the ant colony algorithm to tune the PI controllers at a specific operating point and system parameters to enhance the performance. The DG unit here was represented by constant dc current source. In addition, the ITAE index and THDi index were applied to respectively evaluate the dynamic responses and harmonics. The ITAE and THDi indexes were used as the performance indexes for objective function (OF) of the optimization program.

2. SYSTEM CONFIGURATION

The structure of three-phase four-wire grid-connected inverter for DG application is presented in Figure 1. This figure shows the configuration of grid-connected inverter in which a voltage source inverter acts as a key element of a DG system.

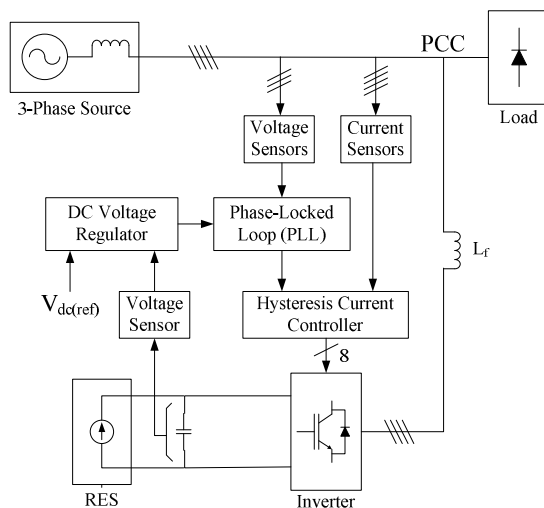


Figure 1: System Configuration

The inverter delivered power from renewable energy source (RES) to grid and solved the quality problem. The four-leg inverter was used to compensate the neutral current of network. This inverter was coupled at the point of common coupling (PCC) via coupling inductance. The switching pulses for the gate drives of inverter were generated by hysteresis current controller. In this system, current source was used to represent the

RES. On the other side, the RES might be an AC source with rectifier.

The control scheme comprised three main components: DC voltage regulator, phase-locked loop and hysteresis current controller. DC voltage regulator was applied to regulate the exchange of active power between RES and grid. Meanwhile, phase-locked loop (PLL) was to track the phase of voltage and hysteresis current controller was used to generate the switching pulses of IGBT.

2.1 DC Voltage Regulator

The DC voltage was regulated to be constant. Through this DC voltage regulator, the power flow in the grid system was regulated. A PI controller was implemented in DC voltage regulator to generate a reference peak current for grid. The dc-link voltage error was obtained by:

$$V_{dc(err)} = V_{dc(ref)} - V_{dc} \quad (1)$$

This error was given to a PI regulator to maintain a constant dc-link voltage. The output of DC voltage regulator was current I_m , - a peak value of reference current flowing in the grid. This current was then be synchronized with the grid voltage through PLL. Figure 2 presents the block diagram of DC voltage regulator.

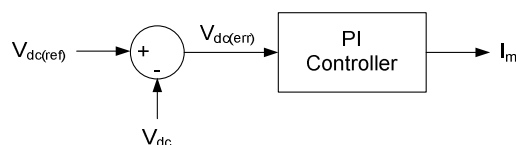


Figure 2: Block Diagram of DC Voltage Regulator

2.2 Phase-Locked Loop

The phase-locked loop (PLL) technique has been used as a common way of recovering the phase and frequency information in electrical systems. In this study, it was used to generate the current references synchronized with the grid voltages. Figure 3 shows the basic configuration of the PLL system.

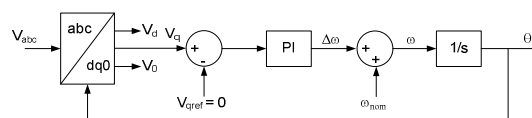


Figure 3: Configuration of the PLL

The PLL used the grid voltage vector $[v_a \ v_b \ v_c]^T$, transformed into the d-q frame. The quadrature voltage component v_q was regulated to zero using a PI controller. The controller output was the grid

voltage angular frequency ω that after integration provided the grid voltage phase θ . In this system, the grid voltage can be expressed as:

$$v_{abc} = V_m \left[\cos(\theta) \quad \cos\left(\theta - \frac{2\pi}{3}\right) \quad \cos\left(\theta + \frac{2\pi}{3}\right) \right]^T \quad (2)$$

where $v_{abc} = [v_a \ v_b \ v_c]^T$. Equation (2) can be expressed in a synchronous reference frame as:

$$v_{dq0} = T(\hat{\theta}) v_{abc} \quad (3)$$

where $v_{dq0} = [v_d \ v_q \ v_0]^T$ and $T(\hat{\theta})$ denotes the matrix given by:

$$T(\hat{\theta}) = \frac{2}{3} \begin{bmatrix} \cos \hat{\theta} & \cos\left(\hat{\theta} - \frac{2\pi}{3}\right) & \cos\left(\hat{\theta} + \frac{2\pi}{3}\right) \\ \sin \hat{\theta} & \sin\left(\hat{\theta} - \frac{2\pi}{3}\right) & \sin\left(\hat{\theta} + \frac{2\pi}{3}\right) \\ \frac{1}{2} & \frac{1}{2} & \frac{1}{2} \end{bmatrix} \quad (4)$$

The instantaneous values of reference three-phase grid currents were then computed as

$$I_a^* = I_m \cdot \cos(\theta) \quad (5)$$

$$I_b^* = I_m \cdot \cos(\theta - 120^\circ) \quad (6)$$

$$I_c^* = I_m \cdot \cos(\theta - 240^\circ) \quad (7)$$

The reference current for the grid neutral current was considered as zero and expressed as

$$I_n^* = 0 \quad (8)$$

2.3 Hysteresis Current Controller

In addition to its function as a power converter to inject power to the system, inverter also acts as a shunt active power filter. Hysteresis current controller acts to generate the switching pulses of IGBT. The actual currents are compared with their reference currents with a predefined hysteresis band. The switching pattern of IGBT can be explained as:

If $(I_a^* - I_a) = +h_b$, then upper switch S_1 will be ON and lower switch S_4 will be OFF in the phase "a" leg of inverter.

If $(I_a^* - I_a) = -h_b$, then upper switch S_1 will be OFF and lower switch S_4 will be ON in the phase "a" leg of inverter.

where h_b is the width of hysteresis band. Similarly, switching pulses for other three legs can be derived.

3. PARAMETER OPTIMIZATION

Parameters K_p and K_i in DC voltage regulator are the optimized parameters. Selecting the best value for these parameters bring some significant effects on controller operation. The selection of these parameters is varied in ways such as trial and error method, Ziegler-Nichols, or intelligent systems. Ant colony optimization (ACO) algorithm is one of the intelligent systems that can be applied to the controller and searches for the optimal values of gains.

3.1 Ant Colony Optimization (ACO) Algorithm

The method of ant colony optimization (ACO) is inspired by the behavior of real ants in finding paths from the colony to the food. The route is taken as optimization parameters K_p and K_i . The number of routes is a parameter entered at the beginning of the simulation. The initial values of variables used for the algorithm are determined by trial and error as shown in Table 1.

Table 1: Initial Values of Parameter in ACO

Ant Number	:	15
Maximum Iteration	:	30
Coefficient ρ	:	0.3
Coefficient c	:	2
Range of parameter (K_p and K_i)	:	0 - 10
$\Delta K_p, \Delta K_i$:	1

3.2 Objective Function

Heuristic methods such as genetics algorithm, particle swarm optimization (PSO), and ACO use objective function for the optimization process. This paper used integral time absolute error (ITAE) of dc-link voltage and average THD of grid currents ($THDi_{ave}$) as the objective function to obtain the optimal parameters of the PI controller K_p dan K_i in DC voltage regulator. $THDi_{ave}$ was the average of $THDi$ phase a, phase b, and phase c. Objective function (OF) for this optimization is presented below.

$$OF = \text{Min}(C_1 \times ITAE + C_2 \times THDi_{ave}) \quad (9)$$

where

$$ITAE = \int_0^t |e_r(t)| \cdot t dt = \int_0^t |V_{dc(ref)} - V_{dc}(t)| \cdot t dt$$

$$THDi_{ave} = \frac{THDi_a + THDi_b + THDi_c}{3}$$

$$C_1, C_2 = \text{constant}$$

$$t = \text{time}$$

It is possible to change the importance of some criteria and events in optimization problem. The value of the constant C_1 and C_2 decides which event is more important from a control design point of view, and which criteria in a particular event should be emphasized. The values of K_p and K_i for which the corresponding objective function is minimum were taken as the optimized gain values.

4. SIMULATION RESULTS AND ANALYSIS

Simulations studies were performed to predict the performance of the proposed method. The parameters selected for simulation studies are presented in Table 2.

Table 2: System Parameters

3-phase Supply (r.m.s)	: $V_g=380$ V, 50 Hz
Source Inductance	: $L_g=1$ mH
DC-Link Capacitance & Voltage	: $C_{dc}=3$ mF, $V_{dc}=750$ V
Coupling Inductance	: $L_{sh}=2$ mH

The load used for generating harmonics and imbalance was composed of: a) a three-phase full wave diode rectifier feeding an RL network consisting of $R_1 = 10 \Omega$ and $L_1 = 10$ mH, b) a three-phase balanced load consisted of $R_A = R_B = R_C = 5 \Omega$ and $L_A = L_B = L_C = 5$ mH, and c) a single phase load in phase A consisted of $R_{AN} = 15 \Omega$ and $L_{AN} = 10$ mH.

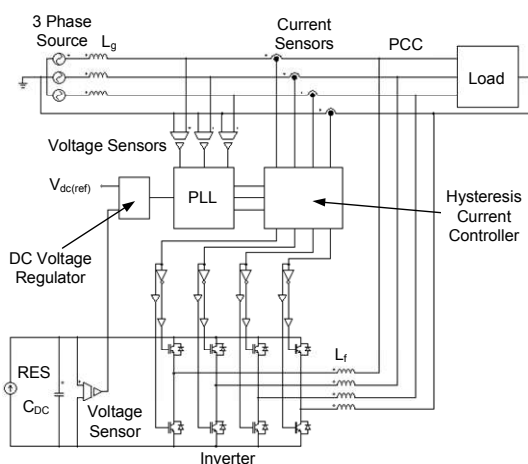


Figure 4: Simulation Block

Figure 4 shows the simulation block of the designed system. A four-leg current was controlled to achieve balanced sinusoidal grid currents with unity power factor. Ant colony optimization algorithm was simulated in Matlab[®] M-File.

4.1 Results

Three case studies including case 1 ($C_1 = 1, C_2 = 0$), case 2 ($C_1 = 0, C_2 = 1$), and case 3 ($C_1 = C_2 = 0.5$) have been studied in this research. The system was turned on at $t = 0$ s and simulation ran until $t = 0.2$ s. Figure 5 shows the fitness curve for case 1, case 2, and case 3. Optimization calculations for case 1 and case 2 achieved convergent on the 14th iteration while case 3 was on the 15th iteration.

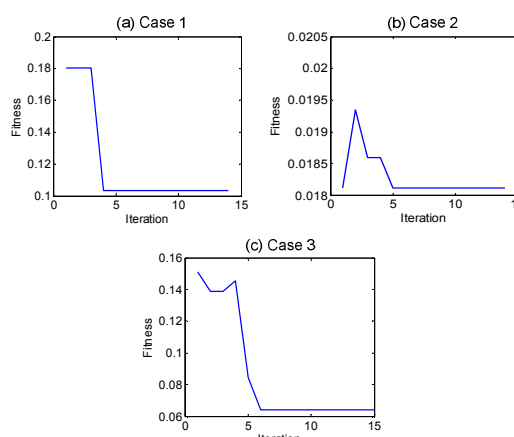


Figure 5: Fitness Curve

Table 3 presents the comparison of the value of system indexes. Optimization for case 1 and case 3 produced the comparable parameter values (K_p and K_i). As seen Table 3, the ITAE for case 2 (0.3274) was about three times higher compared to the one in case 1 (0.1033). However THDi value was almost equal for both cases. Because the weight given to ITAE and THDi in case 3 was equal ($C_1 = C_2 = 0.5$), the result of optimization for case 3 was then closer to the result for case 1.

Table 3: Comparison of Indexes

Parameter and indexes	Non optimized	Optimized		
		Case 1	Case 2	Case 3
K_p	5	2	1	2
K_i	5	6	10	6
ITAE	0.8871	0.1033	0.3274	0.1033
THDi _{ave}	0.0401	0.0247	0.0181	0.0247
Iteration	-	14	14	15

4.2 Analysis

Simulations in this research were conducted to test the system for 0.3 s to determine the performance of the control system. Three different operating conditions were included: (a) $t_A = 0 - 0.1$

s in which switching pulses of IGBT were blocked making the inverter not working; (b) $t_B = 0.1 - 0.2$ s in which the inverter functioned but without any power injection from RES. This made the inverter only functioning as an active power filter; and (c) $t_C = 0.2 - 0.3$ s in which the inverter worked and RES injected power to grid, thus inverter played two functions both as a converter to inject power and as an active power filter.

Figure 6 shows the waveforms for $K_p = 5$ and $K_i = 5$ (non optimized case). Figure 6(a) shows that load currents were unbalanced and non sinusoidal. When $t = 0 - 0.1$ s, the inverter did not function, thus making the grid currents unbalanced and non sinusoidal. At $t = 0.1$ s, average THDi of grid currents was at 9.623 %.

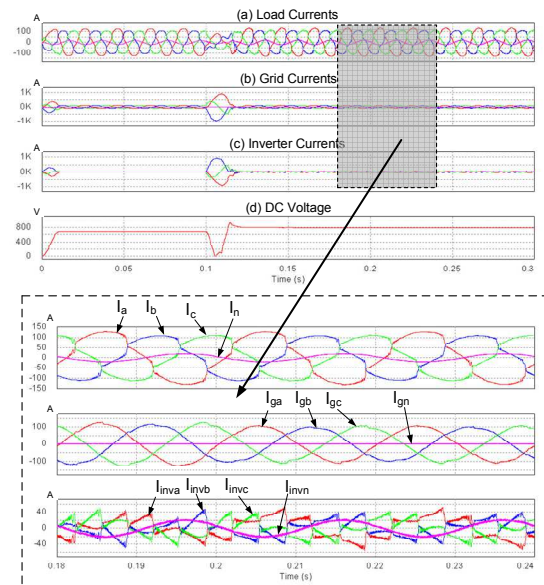


Figure 6: Waveforms for $K_p = 5$ and $K_i = 5$ (non Optimized Case)

As shown in Figure 6(c), the inverter starts working to compensate load current harmonic, load reactive power, and current unbalance at $t = 0.1$ s. In Figure 6(a), the load currents (I_a, I_b, I_c) are non-sinusoidal and neutral current (I_n) flowing due to nonlinearities load. By contrast, the grid currents (I_{ga}, I_{gb}, I_{gc}) as shown in Fig. 6(b) remain sinusoidal. There is no current in the grid neutral current (I_{gn}). Fig. 6(c), meanwhile, shows inverter currents ($I_{inva}, I_{invb}, I_{invc}, I_{invn}$). The load neutral current (I_n) will be supplied through the fourth leg of inverter.

Figure 6(d) shows that DC voltage decreased for $0.1 - 0.12$ s, but after $t = 0.12$ s, this voltage increased to a voltage about 800 V and

subsequently turned slowly into 750 V. At $t = 0.2$ s, the DC voltage was 787.3 V. For $t = 0.1 - 0.2$ s, grid current to be balanced and $THDi_{ave}$ decreased. At $t = 0.2$ s, $THDi_{ave}$ of grid currents was at 3.703 %. At $t = 0.2$ s, RES started injecting power. Figure 6(b) shows that the grid currents slightly decreased after $t = 0.2$ s. As shown in Figure 6(d), DC voltage did not change significantly at $t = 0.2$ s. Average THD of grid current was at 4.103 % at 0.3 s.

Figure 7 shows the grid voltage and current in phase showing the achievement of unity power factor (UPF). It is then proven that inverter could be used to compensate load reactive power demand. Power factor (PF) prior to compensation at 0.95 came to be at 0.99 after compensation.

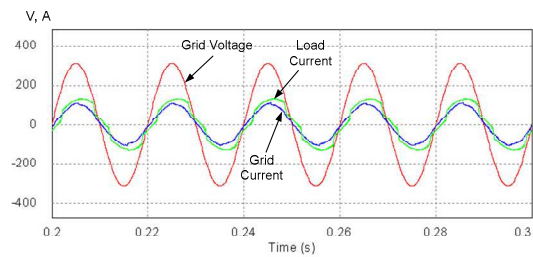


Figure 7: Grid Voltage, Grid Current, and Load Current

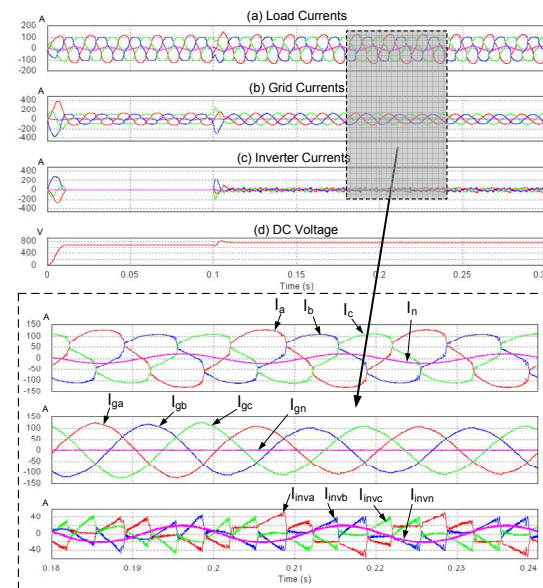


Figure 8: Waveforms for $K_p = 2$ and $K_i = 6$ (Optimized Case 1 and Case 3)

For the case optimization, Figure 8 shows the waveforms for $K_p = 2$ and $K_i = 6$ (case 1 and case 3). Compared with the case without optimization ($K_p = 5$ and $K_i = 5$), the harmonic values at $t = 0.2$ s and $t = 0.3$ s were lower. $THDi_{ave}$ was at 2.208 % at 0.2 s and 2.427 % at 0.3 s. At $t = 0.1$ s, when

inverter started functioning, DC voltage immediately increased to above 750 V and quickly dropped back to 750 V. As shown in Figure 8(b), grid current slightly decreased at 0.2 s because RES started injecting power. Figure 8(d) shows that DC voltage also slightly increased as RES started injecting power.

Figure 9 shows the waveforms for $K_p = 1$ and $K_i = 10$ (optimized - case 2). For these parameters, the $THDi_{ave}$ was the lowest when compared with the case without any optimization ($K_p = 5$ and $K_i = 5$) and optimization case 1 and case 3 ($K_p = 2$ and $K_i = 6$). $THDi_{ave}$ was at 1.662 % at 0.2 s and at 1.990 % at 0.3 s. As shown in Figure 9(d), DC voltage slightly increased when the inverter started working at $t = 0.1$ s and when RES started injecting power at $t = 0.2$ s. DC voltage was 745.7 V at $t = 0.2$ s and 755.1 V at 0.3 s.

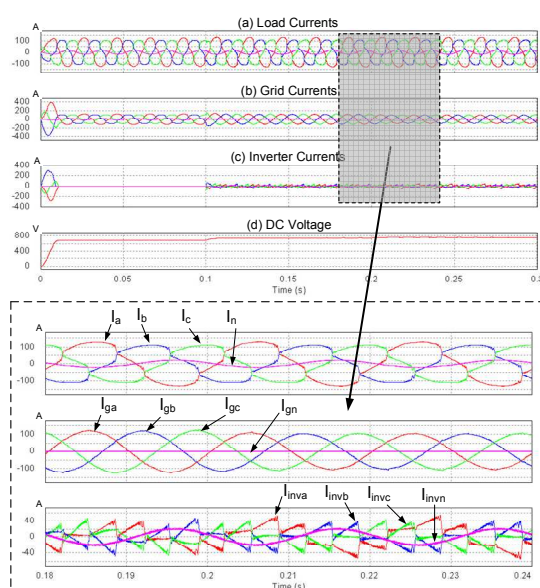


Figure 9: Waveforms for $K_p = 1$ and $K_i = 10$ (Optimized Case 2)

The resume of simulation results are listed in Table 4, showing $THDi_{ave}$ and DC voltage at $t = 0.1, 0.2,$ and 0.3 seconds.

These results indicated that the best harmonic was obtained from optimization case 2. For the response of DC voltage, optimization produced a better performance compared to the one minus optimization. At $t = 0.2$ s, the DC voltage in case 1 and case 3 (751.9 V) was closest to the reference DC voltage (750 V). However at $t = 0.3$ s, the DC voltage for all optimization cases discussed were almost equal.

Table 4: Resume of Simulation Results

Result	Non optimized	Optimized		
		Case 1	Case 2	Case 3
$THDi_{ave}$ (%)				
t = 0.1 s	9.623	9.623	9.623	9.623
t = 0.2 s	3.703	2.208	1.662	2.208
t = 0.3 s	4.103	2.427	1.990	2.427
V_{dc} (V)				
t = 0.1 s	684.6	684.6	684.6	684.6
t = 0.2 s	787.3	751.9	745.7	751.9
t = 0.3 s	774.8	755.9	755.1	755.9

5. CONCLUSION

This paper has presented the parameter optimization of PI controller of grid-connected inverter for DG application to enhance the power quality at PCC. The inverter was utilized to inject power generated from RES to PCC and operated as a shunt active power filter.

The optimization of PI parameters could be used to improve dynamic response and THDi. In this case, parameters K_p and K_i obtained by minimizing ITAE were different from the one obtained by minimizing THDi.

Optimization by means of ACO required a quite long time. However, when compared with other heuristic methods such as genetic algorithms and PSO, this algorithm was still faster. In future, the research will continue with the optimization of grid-connected inverter parameters for DG application based on fuzzy logic control.

REFERENCES:

- [1] Espi, J.M., Castello, J., García-Gil, R., Garcera, G., Figueres, E., "An Adaptive Robust Predictive Current Control for Three-Phase Grid-Connected Inverters", *IEEE Transactions on Industrial Electronics*, Vol. 58, No. 8, 2011, pp. 3537-3548.
- [2] Fanbo He, Zhengming Zhao, Ting Lu, Liqiang Yuan, "Predictive DC Voltage Control for Three-phase Grid-connected PV Inverters Based on Energy Balance Modeling", *2nd IEEE International Symposium on Power Electronics for Distributed Generation Systems (PEDG)*, June 16-18, 2010, pp. 516-519.
- [3] Mosazadeh, S.Y., Fathi, S.H., Hajizadeh, M., Sheykholeslami, A.R., "Adaptive Hysteresis Band Controlled Grid connected PV System with Active Filter Function", *International Conference on Power Engineering and*

- Renewable Energy (ICPERE)*, July 3-5, 2012, pp. 1-8.
- [4] Singh, B., Shahani, D.T., Verma, A.K., "Power Balance Theory Based Control of Grid Interfaced Solar Photovoltaic Power Generating System with Improved Power Quality", *IEEE International Conference on Power Electronics, Drives and Energy Systems (PEDES)*, December 18-19, 2012, pp. 1-7.
- [5] Singh, M., Khadkikar, V., Chandra, A., Varma, R.K., "Grid Interconnection of Renewable Energy Sources at the Distribution Level with Power-Quality Improvement Features", *IEEE Transactions on Power Delivery*, Vol. 26, No. 1, 2011, pp. 307-315.
- [6] Ilavarasi, V., Rajan, C.C.A., "Power Quality Improvement in Grid connected System using Four Leg VSI", *International Conference on Advances in Engineering, Science and Management*, March 30-31, 2012, pp. 540-546.
- [7] Xiaoyong Zhang, Jun Wang, Chuan Li, "Three-Phase Four-Leg Inverter Based on Voltage Hysteresis Control", *International Conference on Electrical and Control Engineering (ICECE)*, June 25-27, 2010, pp. 4482-4485.
- [8] Singh, R., Singh, A.K., Kumar, P., "Comparison of three evolutionary algorithms for harmonic mitigation using SAPF", *6th IEEE International Conference on Industrial and Information Systems (ICIIS)*, August 18-19, 2011, pp. 392-397.
- [9] Yiguang Chen, Xin Gu, Yonghuan Shen, Shengzhi Xing, "Optimization of Active Power Filter System PI Parameters Based on Improved Ant Colony Algorithm", *Proceedings of the 2006 IEEE International Conference on Mechatronics and Automation*, June 25-28, 2006, pp. 2189-2193.
- [10] Yao Shujun, Hu Yanan, Bao Mingran, Han Minxiao, "Parameter optimization of PI controller in PV inverter", *2nd IET Renewable Power Generation Conference (RPG)*, September 9-11, 2013, pp. 1-4.
- [11] Al-Saedi, W., Lachowicz, S.W., Habibi, D., "An optimal current control strategy for a three-phase grid-connected photovoltaic system using Particle Swarm Optimization", *IEEE Power Engineering and Automation Conference (PEAM)*, September 8-9, 2011, pp. 286-290.
- [12] Hassan, M.A., Abido, M.A., "Dynamic performance improvement of an inverter-based grid-connected microgrid", *International Conference on Renewable Energy Research and Applications (ICRERA)*, October 20-23, 2013, pp. 522-527.